Numerical Simulation of Hypersonic Air Intake Flow in Scramjet Propulsion

Sarah Frauholz⋆*, Birgit Reinartz*⋆⋆*, Siegfried Müller*⋆⋆⋆ *and Marek Behr*⋆⋆⋆⋆
⋆*Research Fellow, Chair for Computational Analysis of Technical Systems (CATS), Center for Computational Engineering Science (CCES).*
⋆⋆*Research Associate, CATS, CCES.*
⋆⋆⋆*Professor, Institut für Geometrie und Praktische Mathematik (IGPM).*
⋆⋆⋆⋆*Professor, CATS, CCES.*
RWTH Aachen University, 52056 Aachen, Germany

Abstract

Within this paper, the performance of a scramjet intake is analysed using three-dimensional high-resolution simulations. A mesh-adaptive Reynolds-averaged Navier-Stokes solver is used with the shear stress transport turbulence model. A comparison to published experimental results at $M_\infty = 7$ test condition shows a good overall agreement. Furthermore, the inlet behaviour under flight conditions and for various wall temperatures is studied with respect to the combustor interface.

1. Introduction

Within the frame of the German Research Training Group GRK 1095 "Aero-Thermodynamic Design of a Scramjet Engine for Future Space Transportation Systems", a combined numerical and experimental analysis of hypersonic air intake flow in Scramjet propulsion is being conducted.

The intake of a supersonic combustion Ramjet (Scramjet) consists mostly of several exterior compression ramps followed by an interior part. Oblique shock waves generated by the ramps and the cowl lip are performing the compression of the incoming flow. To protect the pressure-sensitive intake from the back pressure of the combustion chamber, an isolator is used. There, the flow adapts to the back pressure using a shock train. Multiple interesting as well as physically complex phenomena may occur, such as shock-boundary layer interaction, laminar-turbulent transition and compressible relaminarization.

A fully three-dimensional intake has been designed at the German Aerospace Center (DLR) in Cologne. A first test campaign has been performed 2012 and a second test campaign is planned for 2013. Since experimental measurements are very costly and difficult to perform, numerical computations are necessary to analyse and understand the flow phenomena. Thus, a numerical analysis in cooperation with the German Aerospace Center Cologne is performed.

For this purpose an in-house code QUADFLOW is used. This solver is an h-adaptive and fully implicit flow solver for the Reynolds-averaged Navier-Stokes equations for compressible flow using a fully unstructured cell-centered finite volume method. It follows an integrated concept of surface-based discretization, multiscale analysis, and, on this basis, an h-adaptive grid generation applying B-spline techniques.

The paper presents the ongoing work. Several three-dimensional simulations of the new scramjet intake at wind tunnel and flight condition are shown. First, one computation with wind tunnel condition is performed to generate data in comparison to the experimental measurements. In cooperation with the Institute of Aerospace Thermodynamics (ITLR), University of Stuttgart, we also investigate the interaction with the combustor. At the ITLR, computations for the combustion chamber are performed. This work provides the input data by extracting data at the interface of the intake and combustor. With respect to combustion simulations, flight conditions have to be used, because the pressure and temperature level required for combustion are not reached in the wind tunnel facility. Within this paper, the difference between the two conditions is discussed. Then three computations at flight condition with increasing wall temperature are performed focusing on the impact of the wall temperature.

2. Experimental Settings

The geometry of the considered Scramjet intake is shown in Figure 1. The model is 750 mm long. The ramp angle is 8° and the side wall angle 7° each. The intersection of the ramp and side walls exhibits a smooth curvature. The sweep angle of the side wall is 45° and reduces smoothly downstream. At $x = 650$ mm, the interface of the intake and the combustor is defined. Downstream of this location the walls are divergent by 1°. The intake has a V-shaped lip to take the interaction of the side wall shocks and ramp shock into account. The front part of the cowl is movable. Thus, the lip position can be varied between $x_{lip} = 300$ mm and $x_{lip} = 450$ mm. The fixed part of the cowl starts at $x = 550$ mm.

For all computations within this paper, the lip position is $x_{lip} = 300$ mm which is the condition with maximum internal contraction [7]. For optimal performance, the lip has to be moved further downstream until the shock-on-lip condition is fulfilled.

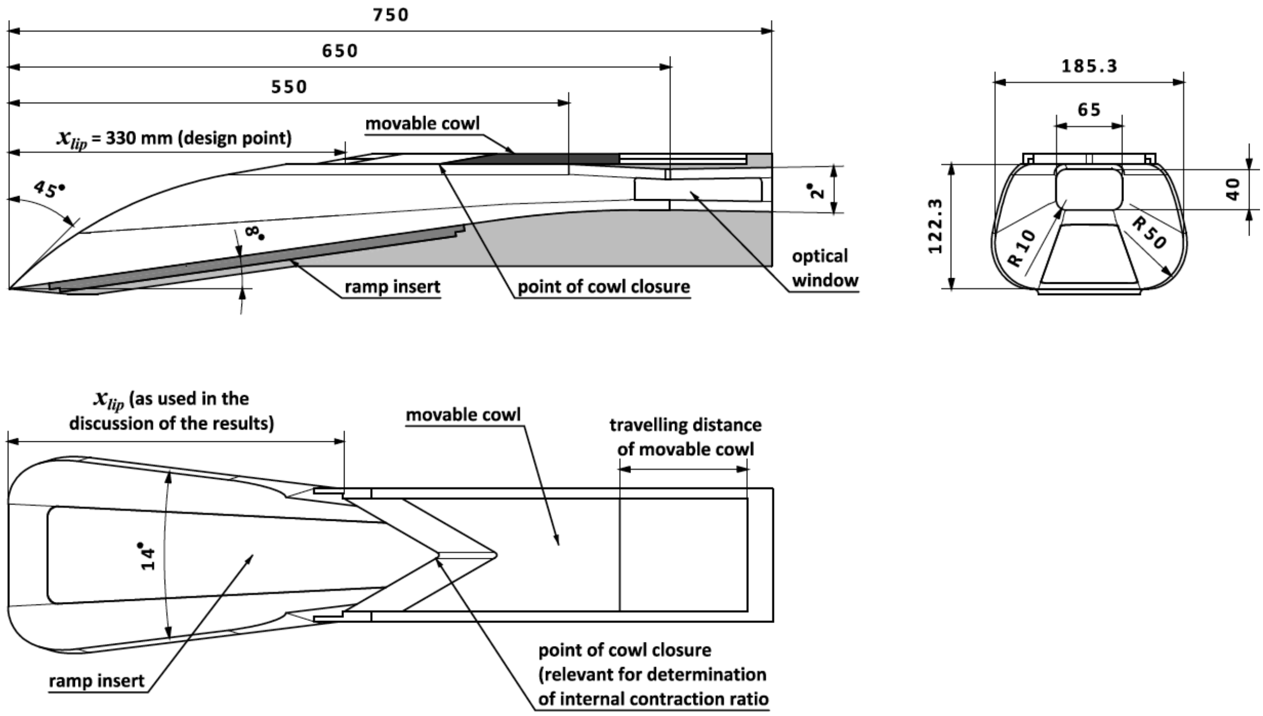

Figure 1: CAD model of the intake. Reproduced from Hohn and Gülhan [7].

The configuration was tested at the Hypersonic Windtunnel H2K at the German Aerospace Center in Cologne. The test conditions in the experiments and the corresponding flight conditions are listed in Table 1. These values are used as inflow conditions in the simulations. During the experiments, the surface pressure in the intake was measured by a total of 55 Kulite pressure probes [7].

Table 1: Wind tunnel conditions and flight conditions for the Scramjet intake configuration

condition	M_∞	Re_∞ **[10^6/m]**	T_0 **[K]**	T_∞**[K]**	T_{wall} **[K]**
wind tunnel	7.0	2.6	700	64.8	300
flight	8.0	2.6	3128	226.65	$[300, 600, 900]$

3. Numerical Method

3.1 Solver QUADFLOW

QUADFLOW is a well validated flow solver which solves the Reynolds Averaged Navier-Stokes equations for unsteady, compressible fluid flow in two and three dimensions [3]. This solver has been developed over a period of more than one decade within the Collaborative Research Center SFB 401 “Flow Modulation and Fluid Structure Interaction at Airplane Wings” and the German Research Training Group GRK 5 “Transport Processes in Hypersonic Flow” at RWTH Aachen University. It has been validated extensively against different test cases [2, 12, 8].

The flow solver is based on a cell-centered finite volume discretization. The mesh is treated as fully unstructured and composed of simply connected elements with otherwise arbitrary topology. For the time and space discretization the user can choose among several options for the Riemann solver, the limiter, the polynomial reconstruction and the Runge-Kutta scheme. Here we summarize the methods used for the computations presented in Section 4. For the discretization of the convective fluxes, the AUSMDV Riemann solver has been used. A linear reconstruction of the primitive variables is performed to locally achieve second order accuracy in space, and the Venkatakrishnan slope limiter is employed to avoid oscillations typical of second-order schemes [13]. For the discretization of the viscous fluxes, a modified central difference method is used. For the time integration, a second order accurate explicit Runge-Kutta scheme is employed. To simulate turbulent flow, a wide variety of low Reynolds number turbulence models for compressible fluid flow are implemented. In this study, we are using the Shear Stress Transport (SST) model.

Quadflow is parallized using MPI and space-filling curves [4, 5]. Within this paper, the three-dimensional computations are performed using 60 processors of the Bull cluster of RWTH Aachen University.

3.2 Boundary Conditions

At the supersonic inflow boundary, the free stream conditions listed in Table 1 are prescribed assuming a turbulence intensity of 0.5%. For the supersonic outflow, the variables are extrapolated from the interior assuming zero gradient. At solid walls, the no-slip condition is enforced by setting the velocity components to zero. Due to the short measurement times in the experiments, the walls are isothermal. For the wind tunnel conditions we also assume isothermal walls. In real flight, the walls will heat up due to thermal loads. To take this into account we vary the wall temperature and analyse its influence.

3.3 Grid Generation

The three-dimensional grid is generated with the commercial program ANSYS ICEM CFD and transformed by GNAGG into a multiblock-structured data format, which is necessary for performing multi-level computations in the flow solver QUADFLOW. GNAGG is an in-house multiblock grid generator providing in each block a grid mapping that implicitly defines the grid hierarchy of the multiscale analysis by uniformly refining the parameter space [9]. Due to the multiblock concept, the discretization of each individual block is as independent as possible.

For the computations, three refinement levels are used. The grid points in wall-normal direction are stretched towards the walls using a Poisson distribution. Transverse to the wall, the grid lines are almost everywhere orthogonal to the walls to resolve the strong wall gradients accurately. To realize individual discretization for different regions, the grid is divided into 92 blocks, which are merged into eight blocks during the grid generation process.
The initial grid on refinement level $L = 1$ consists of 26,400 cells and is shown in Figure 2. The final, uniformly refined grid at refinement level $L = 3$, obtained after two refinement steps, consists of approximately 1,689,600 cells and is presented in Figure 3. The minimum wall distance of the $L = 3$ grid is 3×10^{-6} m.

From former grid convergence studies for similar hypersonic flow problems with different scramjet intakes and compression corners we know that this minimum wall distance is still too large to get grid-converged results. Normally, $y^+ < 1$ is required to produce grid independent results. Therefore, a minimum wall distance of around 10^{-6} m is required. Bosco [1] showed that for hypersonic flows even this spacing is often too large to resolve correctly the strong temperature gradients at the wall. Thus a minimum wall distance of 10^{-7} m or less is suggested.

In general we are aiming to perform mesh-adaptive computations on this geometry since this is a promising approach to save computational costs while maintaining the accuracy of the results. So far, the mesh-adaptive approach was successfully applied to several 2D configurations and to a different three-dimensional scramjet intake [6]. Hence, the computation presented in this paper are part of the progress towards that goal and we do not compute on any higher refinement levels yet.

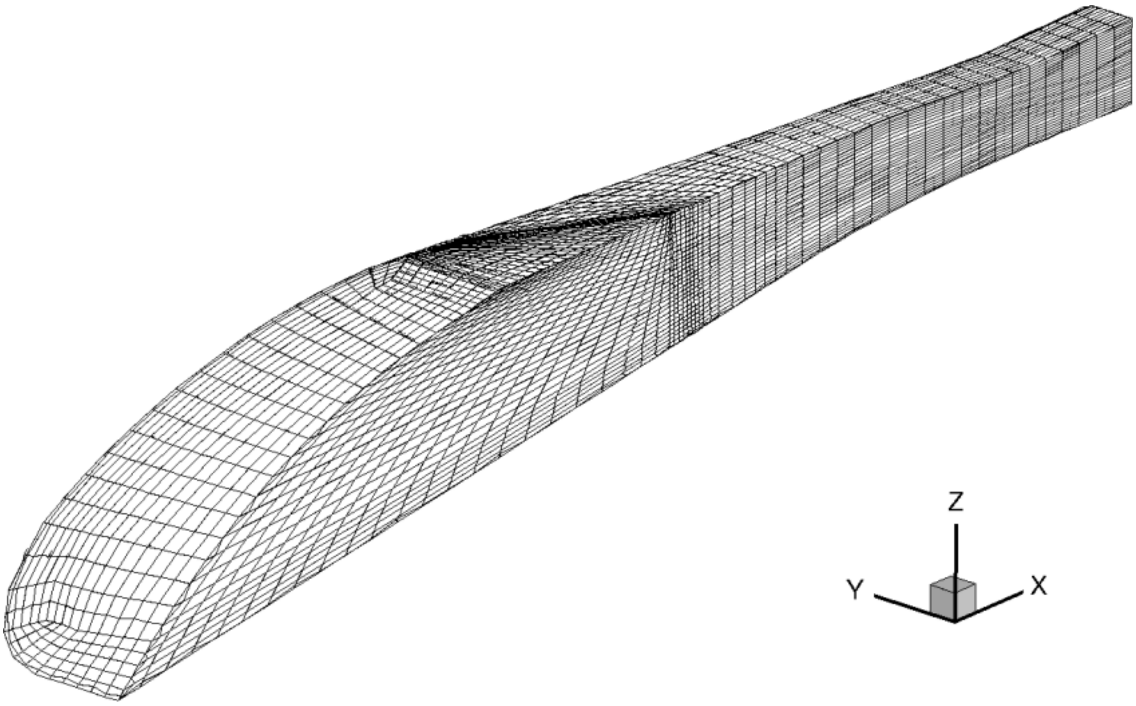

Figure 2: Initial grid on uniform level 1.

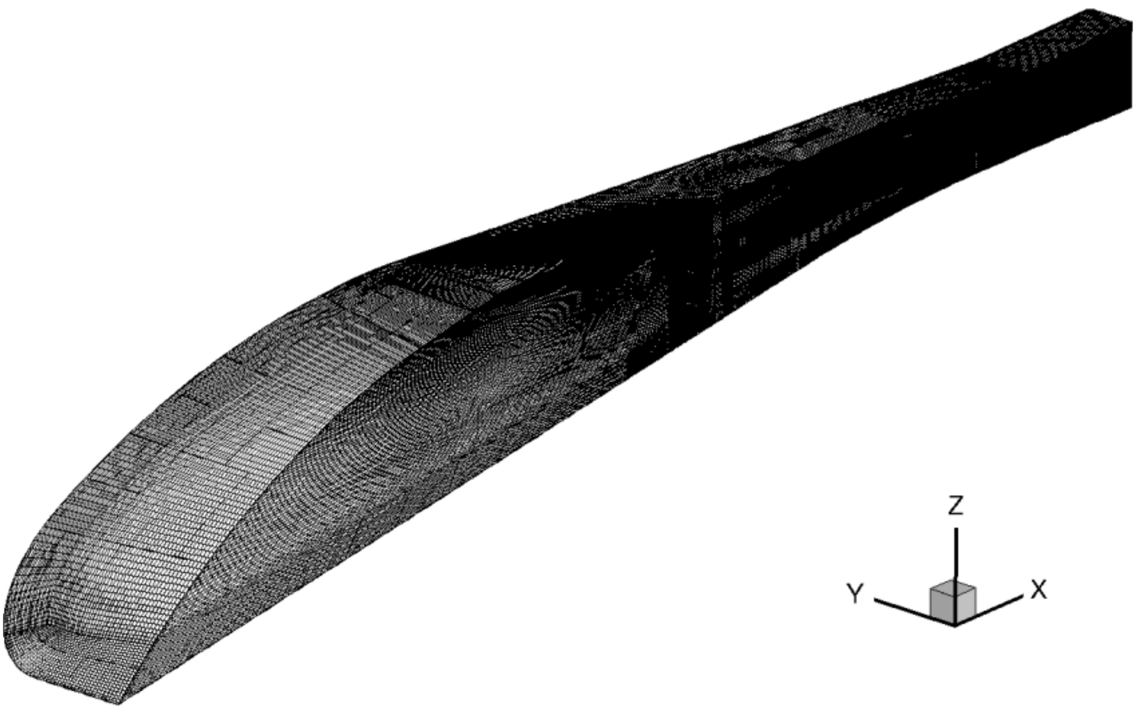

Figure 3: Final grid on uniform level 3.

4. Results

First of all the general flow features for the wind tunnel condition are discussed. Afterwards the flight condition is considered and compared to the wind tunnel condition. Then the influence of the wall temperature is investigated.

4.1 Wind tunnel condition

To illustrate the three-dimensionality of the flow, Figure 4 presents the normalized wall heat flux in terms of the Stanton number at the wall. The Mach number at different cross sections is also shown. The heat load at the exterior portion of the intake is moderate, except for the leading edges of the ramp and the lower side wall. As the flow moves inside the intake, more shock waves are generated by deflection and impinge on the surface, creating several areas of intense heating.

The Mach number plots show the strong interaction of the leading edge shock wave and the side wall shock wave. Both shock waves are of approximately the same strength due to similar deflection angles. In the last cross section a third shock wave, generated by the V-shaped cowl, appears and intensifies the interaction. Thus the flow is highly three-dimensional.

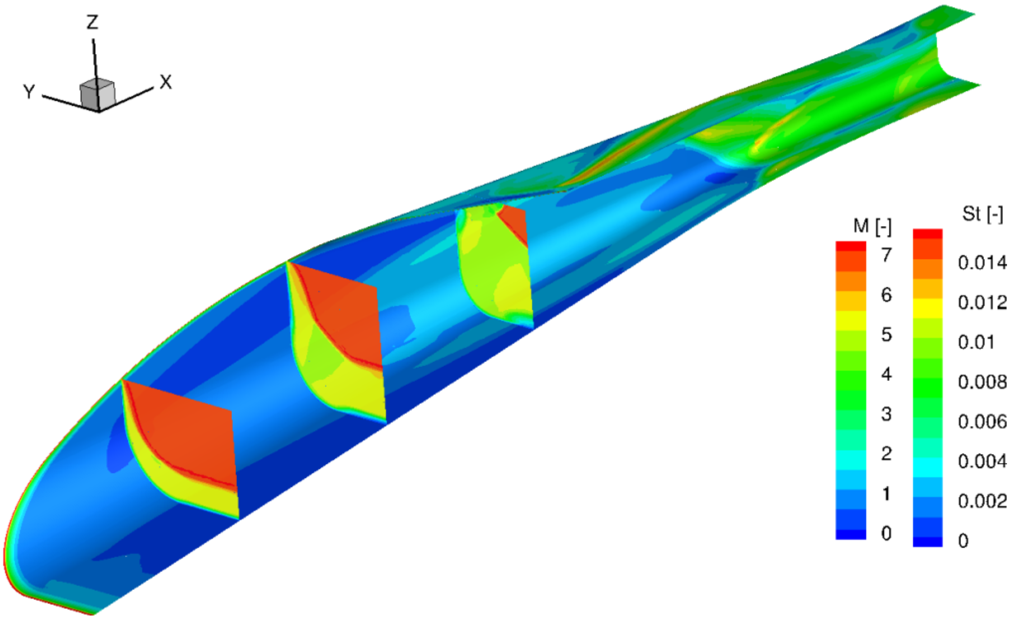

Figure 4: **Mach number distribution at different cross sections of the intake and Stanton number distribution at the intake walls for wind tunnel condition.**

Figure 5 shows the Mach number distribution in the symmetry plane. First the flow is compressed by the leading edge shock (1). At the lower intake wall, a turbulent boundary layer develops and rapidly thickens (3) due to side wall effects and the impinging cowl shock. Note that the boundary layer is fully turbulent in the computation due to the chosen turbulence model. This is done because no information about the location of the laminar-to-turbulent transition is know from the experiments. Outside the boundary layer (2) the flow is not disturbed by the side wall compression. Due to the chosen off-design lip-position, the leading edge shock hits the upper intake wall and interacts there with the lip shock and the boundary layer. The shock-shock-interactions and shock-boundary-layer-interactions (4) result in an oblique shock from the upper intake wall (5). This shock impinges on the thick boundary layer at the lower wall and is reflected. Due to the expansion, the boundary layer thickness decreases (6). At the complete upper intake wall the flow is separated (7).

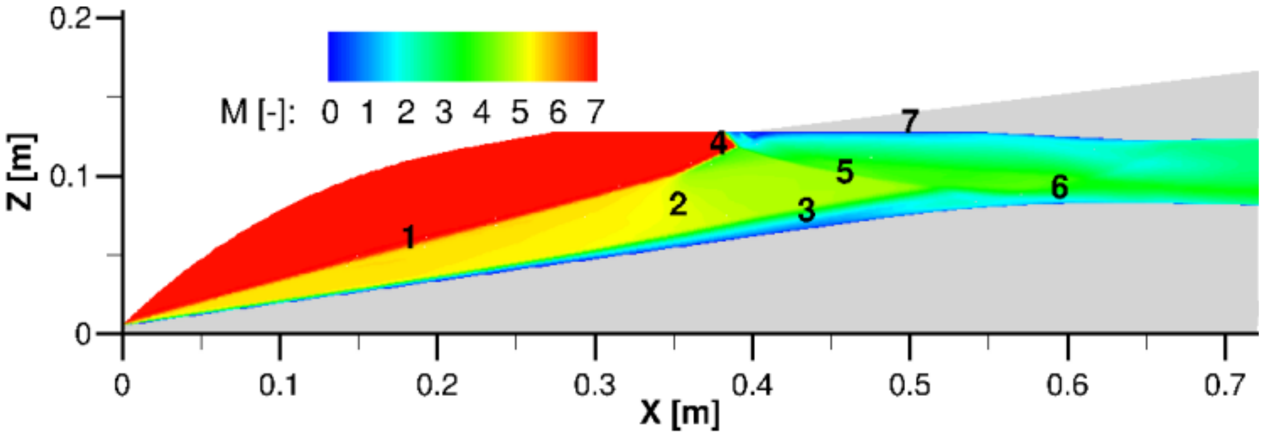

Figure 5: **Mach number distribution in the symmetry plane of the intake for wind tunnel condition.**

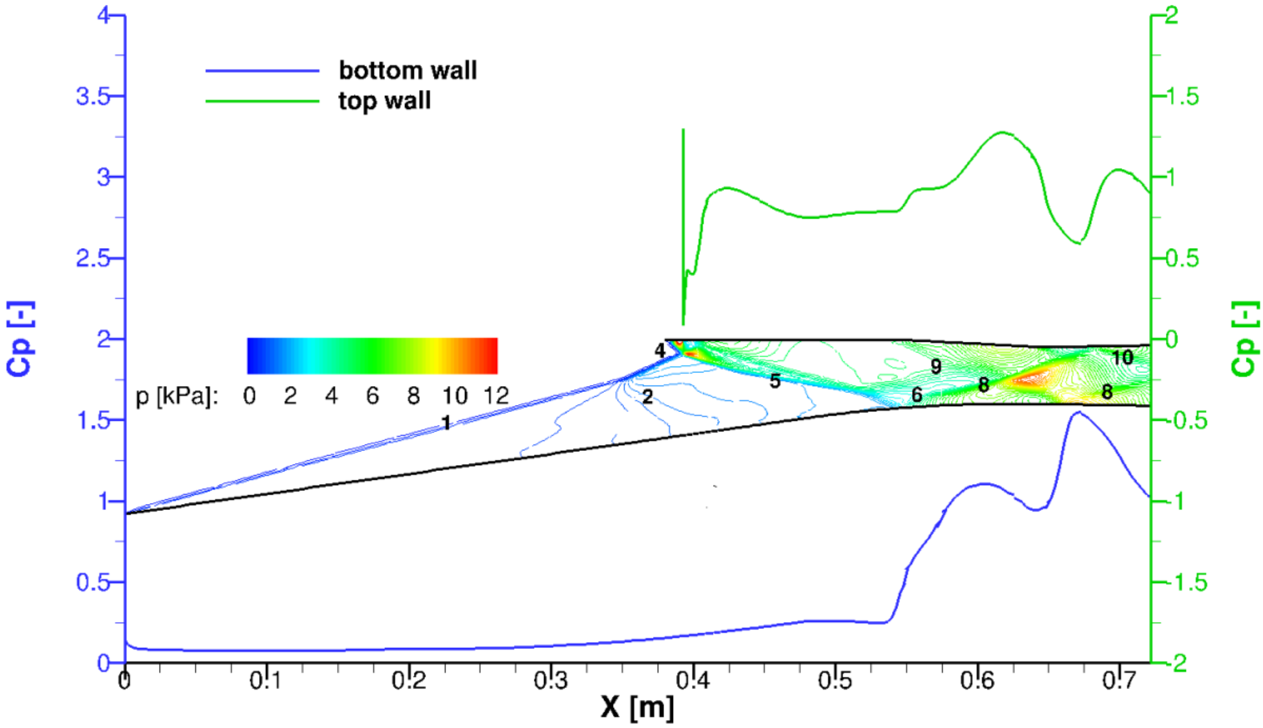

Figure 6: **Wall pressure coefficient distribution along the lower and upper wall of the intake in the symmetry plane and pressure lines in the symmetry plane for wind tunnel condition.**

To analyse the flow further, the distributions of the pressure coefficient :

$$c_p = \frac{p - p_\infty}{\frac{1}{2}\rho_\infty u_\infty^2}, \tag{1}$$

and the Stanton number:

$$St = \frac{q_w}{\rho_\infty \left| u_\infty \right| c_p (T_{0,\infty} - T_w)}, \tag{2}$$

are shown for both intake walls. Figures 6 and 7 show also the pressure distribution and temperature distribution of the intake, respectively. All flow features described above can be identified here as well. They are marked with the same numbers as in the Mach contour, see Figure 5. The leading edge shock is visible in the pressure and temperature lines. Due to the adverse pressure gradient that can be clearly seen in the

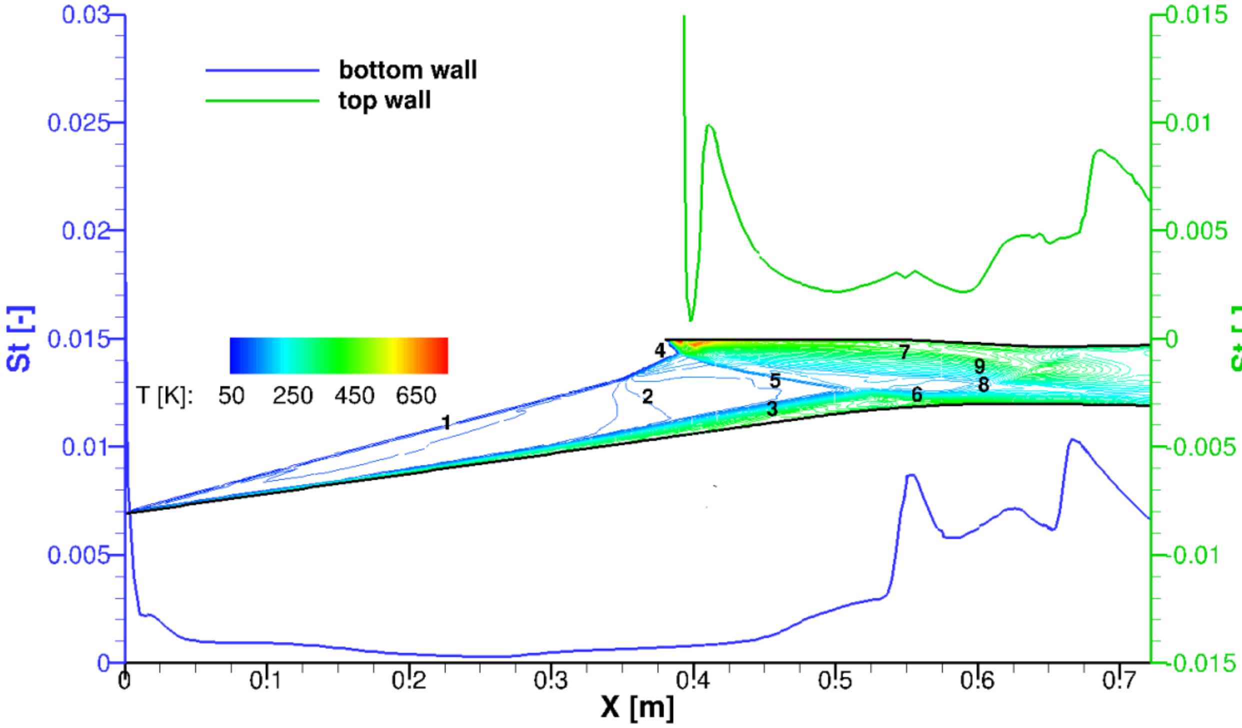

Figure 7: **Stanton number distribution along the lower and upper wall of the intake in the symmetry plane and temperature lines in the symmetry plane for wind tunnel condition.**

pressure coefficient, the boundary layer at the lower intake wall (3) thickens. The thick boundary layer is visible in the temperature plot. At the lower intake wall, the first pressure rise is caused by the cowl shock (5) hitting the wall. At the kink between the movable and fixed part ($x = 550$ mm) of the cowl, an oblique shock (9) occurs and causes the rise of pressure coefficient at the upper intake wall. At the second pressure rise at the lower intake wall shock (9) interacts with the flow at the lower intake wall and is reflected (8). The cowl shock (5) is reflected as well (8). After the interface to the combustor ($x = 650$ mm), the intake divergences slightly and at the upper intake wall, the interaction of the shock reflection and the expansion (10) can be seen. The Stanton number distribution shows the peak heating where the shocks hit the intake wall.

Final comparison with experimental data is still pending, however comparison with the experimental results published in [7] shows an overall good agreement. The wall pressure distributions indicate the same shock locations and the Stanton number distribution derived from IR measurements agree in distribution and value with the computed data presented in Figure 6.

4.2 Flight condition

Figures 8 and 9 show the Mach number contour and the pressure lines for the symmetry plane of the intake for flight conditions with a wall temperature of 300 K, respectively. In contrast to the wind tunnel condition the inflow Mach number and the inflow temperature are higher. Still the main flow phenomena remain the same. The flow features are marked with the same numbers as before. For comparing to the wind tunnel condition, note that the scale of the Mach number and pressure are changed. Due to the higher total temperature the pressure rises above 50 kPa whereas for the wind tunnel condition the maximum pressure is around 12 kPa.

Mainly due to the higher inflow Mach number, the leading edge shock angle is smaller and the leading edge shock (1) hits the upper intake wall further downstream. Thus, the oblique shock wave resulting from the interaction of the leading edge shock wave, the cowl shock wave and the boundary layer (4) occurs further downstream as well. The shock wave (5) hits the lower intake wall and is reflected (8). Since the shock wave (9) is produced by the kink between the moveable part of the cowl and the fixed part of the cowl this shock wave occurs at the same position as before. Due to the different inflow condition resulting in slightly different flow conditions in the interior portion this shock wave (9) hits the lower intake wall close to the end of the

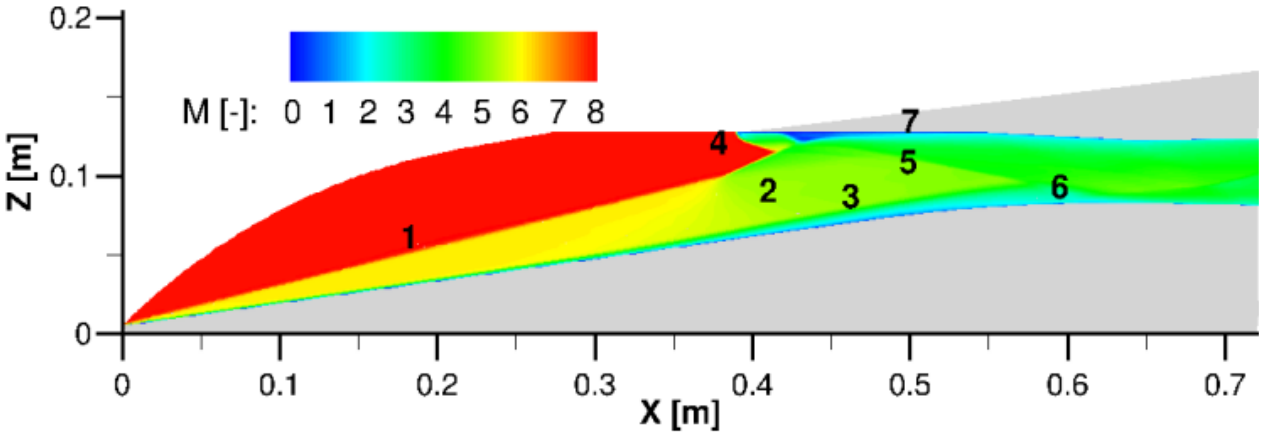

Figure 8: **Mach number distribution in the symmetry plane of the intake for flight condition with wall temperature $T_w = 300$ K.**

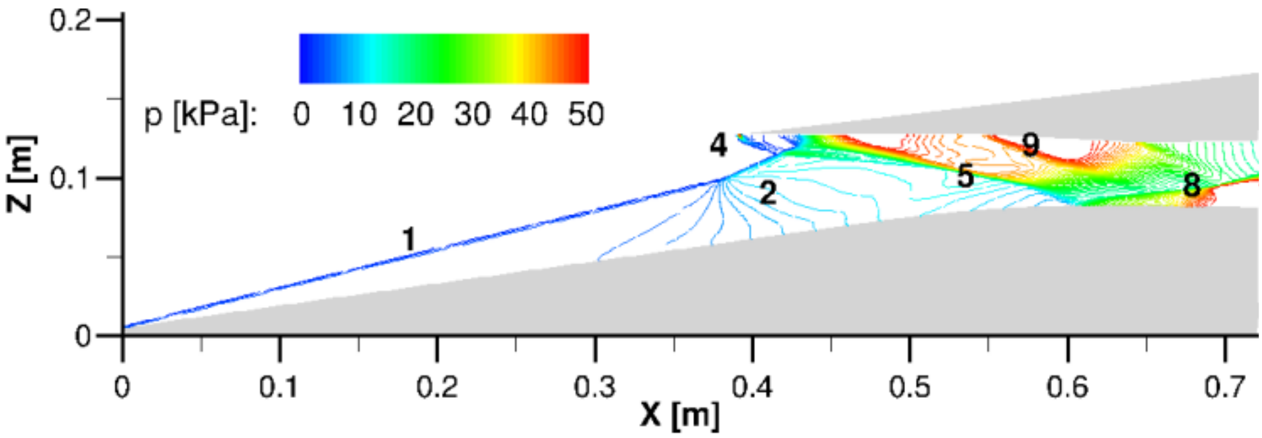

Figure 9: **Pressure distribution in the symmetry plane of the intake for flight condition with wall temperature $T_w = 300$ K.**

computed domain and is reflected there producing a high local pressure.

The change of the position of the shock waves is also clearly visible in the pressure rises and the peak heatings. Figures 10 and 11 show the pressure coefficient and the Stanton number distribution, respectively, at the intake walls in the symmetry plane for the wind tunnel condition as well as the flight condition. Especially positions (a), (d) and (e) are shifted further downstream in case of flight condition. These positions are characterized by impinging shock waves that have different shock angle due to the higher inflow Mach number. Position (b) does not change since the shock wave is generated by the kink in the geometry. The shock reflection (c) is only visible for the lower inflow Mach number at wind tunnel condition. For the $M_\infty = 8$ computation, the shock hits the upper wall behind the intake.

Figure 12 shows the pressure coefficient and Stanton number for different wall temperatures at flight condition. Here one can notice that the influence of the wall temperature is rather small since the effects are blurred by the thick boundary layers. However, for higher wall temperatures most flow features are shifted slightly downstream.

A greater difference can be seen when analysing the cross section flow. This is done for the combustor entrance ($x = 650$ mm). In Figure 13 we present the Mach number, pressure and temperature contours for wall temperature $T_w = 300$ K and $T_w = 900$ K, respectively. The general structure of the flow is the same but the values differ. For wall temperature $T_w = 300$ K, the Mach number in the interior flow is higher than for wall temperature $T_w = 900$ K. Hence, the pressure and temperature are lower for wall temperature $T_w = 300$ K.

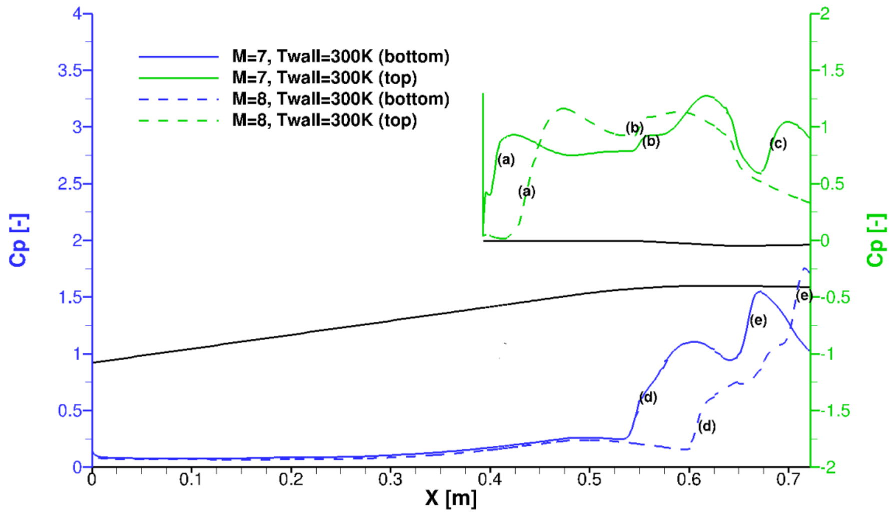

Figure 10: **Wall pressure coefficient distribution along the lower and upper wall of the intake for wind tunnel and flight condition with wall temperature $T_w = 300$ K. Illustration of flow structures: (a) leading edge shock wave hits the wall, (b) shock wave due to geometry change, (c) shock reflection, (d) cowl shock hits the wall and (e) shock reflection.**

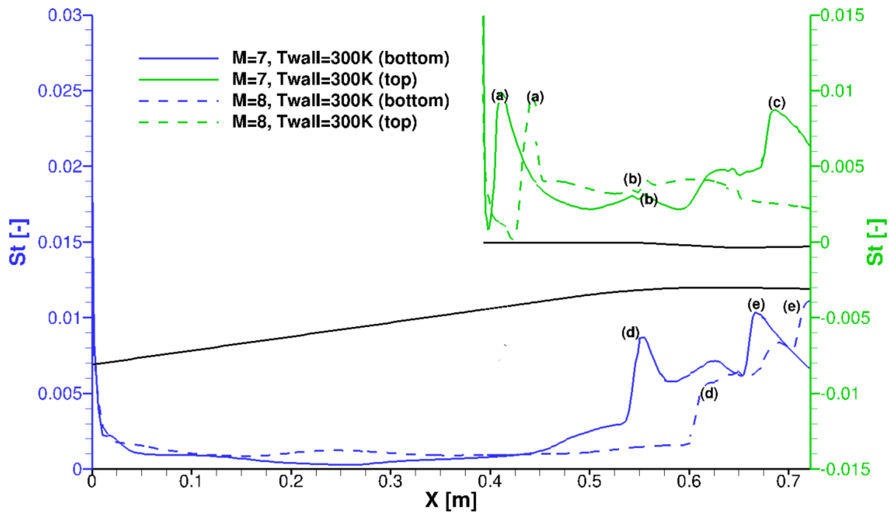

Figure 11: **Stanton number distribution along the lower and upper wall of the intake for wind tunnel and flight condition with wall temperature $T_w = 300$ K. Illustration of flow structures: (a) leading edge shock wave hits the wall, (b) shock wave due to geometry change, (c) shock reflection, (d) cowl shock hits the wall and (e) shock reflection.**

Regarding the interaction with the combustor the computation with higher wall temperature is considered, since during flight the wall heats up. To obtain self-ignited supersonic combustion, at the entrance of the combustor, the Mach number should be sufficiently low and the static temperature should be sufficiently high. In addition a uniform flow field is desirable to stabilize the combustion process. In the middle of the shown cross section the flow is homogeneous in a wide area. Here, the Mach number is still between 3 and 4 and the temperature is between 600 K and 800 K. For stable self-ignition, a static temperature of around 1000 K is necessary. This temperature is reached in the outer regions of the cross section. Since a central struct injector is investigated, the temperature in the middle of the cross section might not be sufficient for stable self-ignition. Comparing to lower wall temperatures, the hot wall helps to increase the temperature and the pressure in the cross section and to decrease the Mach number.

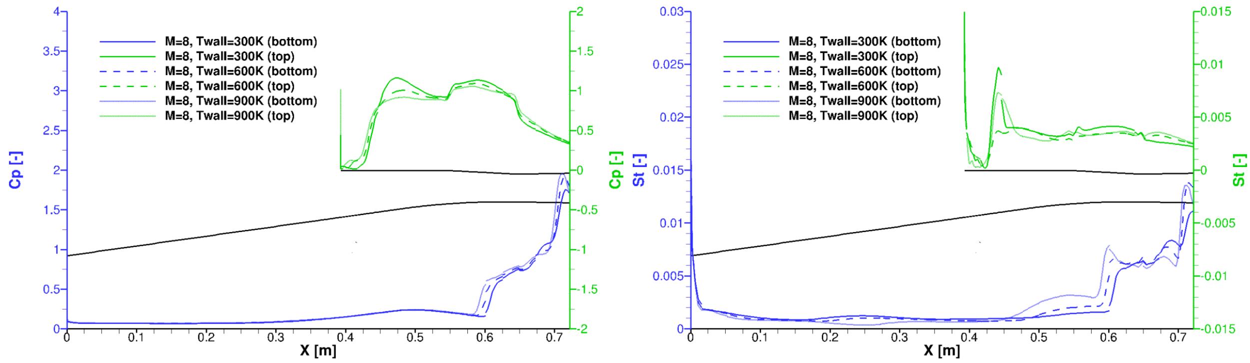

Figure 12: **Wall pressure coefficient distribution (left) and Stanton number distribution (right) along the lower and upper wall of the intake in the symmetry plane for wind tunnel and flight condition with different wall temperatures.**

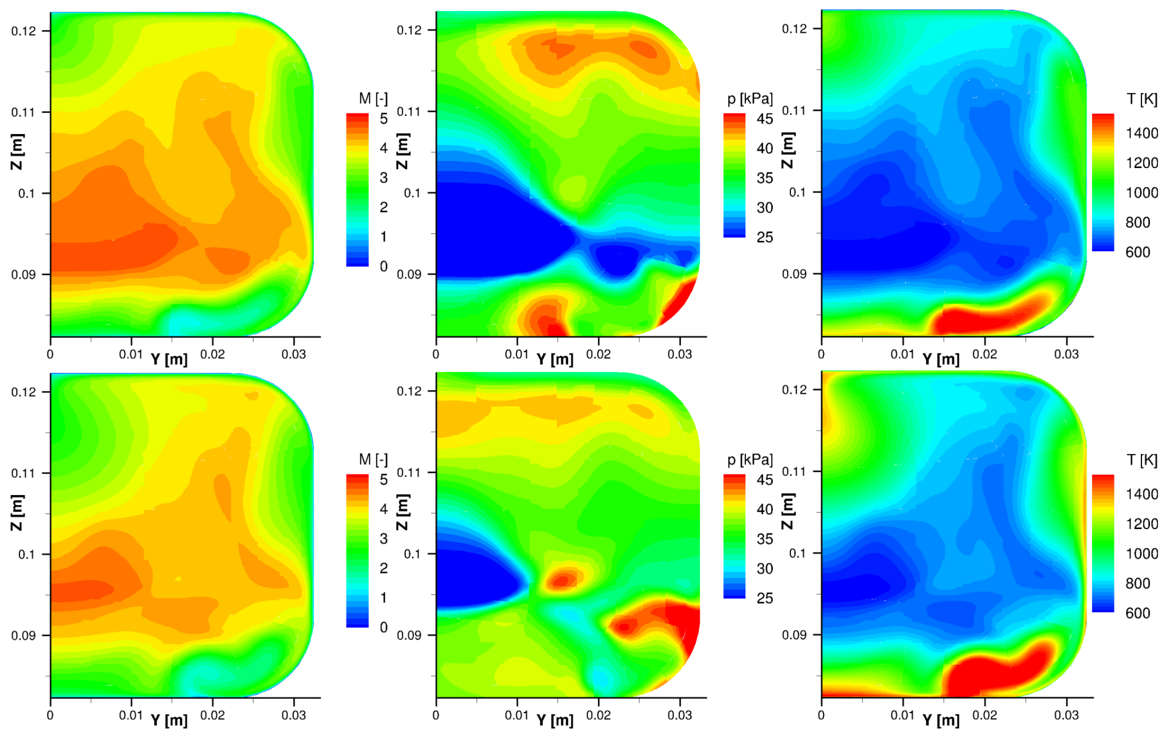

Figure 13: **Mach number (left), pressure (middle) and temperature (right) contours at the entrance plane of the combustor for flight condition with wall temperature $T_w = 300$ K (top) and $T_w = 900$ K (bottom).**

5. Conclusions

First simulation results are presented for the new GRK 1095/2 intake that is currently being tested at the German Aerospace Center (DLR) in Cologne. The simulations show that due to off-design condition with respect to the cowl position, the leading edge shock wave impinges on the underside of the cowl and separates the boundary layer for a large part of the cowl section. Due to similar compression angles on ramp and side walls, the interior flow remains largely homogeneous. Investigations of the combustor entrance plane reveal that the entrance Mach number is still high and, consequently, the temperature might not be sufficient for stable self-ignition.

Acknowledgments

This work was supported by the German Research Foundation (DFG) within the framework of the GRK 1095 "Aero-Thermodynamic Design of a Scramjet Propulsion System for Future Space Transportation Systems". Computing resources were provided by the RWTH Aachen University Center for Computing and Communication and the Research Center Jülich. The experimental data was provided by the German Aerospace Center in Cologne.

References

[1] Arianna Bosco, Birgit Reinartz, Laurie Brown, and Russell Boyce. Investigation of a compression corner at hypersonic conditions using a reynolds stress model. AIAA Paper 2011-2217, April 2011.

[2] F. D. Bramkamp, Ph. Lamby, and S. Müller. An adaptive multiscale finite volume solver for unsteady and steady flow computations. *Journal of Computational Physics*, 197:460–490, 2004.

[3] Frank Bramkamp. *Unstructured h-Adaptive Finite-Volume Schemes for Compressible Viscous Fluid Flow*. PhD thesis, RWTH Aachen University, 2003.

[4] Kolja Brix, Silvia Sorana Melian, Siegfried Müller, and Mathieu Bachmann. Adaptive multiresolution methods: Practical issues on data strucutres, implementation and parallelization. In Violaine Louvet and Marc Massot, editors, *ESAIM Proceedings*, volume 34, pages 151–183, 2011.

[5] Kolja Brix, S. Mogosan, S. Müller, and G. Schieffer. Parallelization of multiscale-based grid adaptation using space-filling curves. In F. Coquel, Y. Maday, S.Müller, M. Postel, and Q.H. Tran, editors, *ESAIM Proceedings*, volume 29, pages 108–129, 2009.

[6] Sarah Frauholz, Marek Behr, and Birgit Reinartz. Numerical simulation of hypersonic air intake flow in scramjet propulsion using a mesh-adaptive approach. In *18th AIAA International Space Planes and Hypersonic Systems and Technologies Conference, Tours, France, 23-27 September 2012, AIAA Paper 2012-5976*, 2012.

[7] Oliver M. Hohn and Ali Gülhan. Analysis of a three-dimensional, high pressure ratio scramjet inlet with variable internal contraction. In *18th AIAA International Space Planes and Hypersonic Systems and Technologies Conference, Tours, France, 23-27 September 2012, AIAA Paper 2012-5975*, 2012.

[8] Martin Krause and Josef Ballmann. Enhanced design of a scramjet intake using two different rans solvers. In *26th International Symposium on Shock Waves, Goettingen (OH), Germany, 15-20 July 2007*, 2007.

[9] Ph. Lamby. *Parametric Multi-Block Grid Generation and Application To Adaptive Flow Simulations*. PhD thesis, RWTH Aachen, 2007.

[10] Siegfried Müller. Adaptive multiscale schemes for conservation laws. In *Lecture Notes on Computational Science and Engineering*, volume 27. Springer-Verlag, 2003.

[11] Siegfried Müller. Multiresolution schemes for conservation laws. In R. DeVore and A. Kunoth, editors, *Multiscale, Nonlinear and Adaptive Approximation*, pages 379–408. Springer-Verlag, 2005.

[12] Tue Nguyen, Gero Schieffer, Christian Fischer, Herbert Olivier, Marek Behr, and Birgit Reinartz. Details of turbulence modeling in numerical simulations of scramjet intake. In *27th Congress of International Council of the Aeronautical Sciences (ICAS), Nice, France, 19-24 September 2010*, 2010.

[13] V. Venkatakrishnan. Convergence to Steady State Solutions of the Euler Equations on Unstructured Grids with Limiters. 118:120–130, 1995.